CFD Calculation of Aerodynamic Indicial Functions for a Generic Fighter Configuration

Mehdi Ghoreyshi, Ph.D., Martiqua L. Post, Ph.D., and Russell M. Cummings, Ph.D.
Modeling and Simulation Research Center,
U.S. Air Force Academy, Colorado

A reduced-order modeling of nonlinear and unsteady aerodynamics based on indicial (step) response functions and Duhamel's superposition integral is presented. These time-domain models could predict the unsteady aerodynamic responses of an aircraft performing any arbitrary motion over a wide range flight regime, but require calculating a large number of response functions. A method to efficiently reduce the number of indicial response calculations is tested. This method uses a time-dependent surrogate model (input/output mapping) to fit the relationship between flight conditions and response functions from a limited number of response simulations (samples). Each sample itself is directly calculated from unsteady computational fluid-dynamic simulations and a grid-motion tool. An important feature of this approach is uncoupling the effects of angle of attack and pitch rate from pitching motions. The aerodynamic models are then created with predicted indicial functions at each time instant using the surrogate model. This model is then applied for aerodynamics modeling of a generic fighter configuration performing arbitrary pitching and plunging motions at various Mach numbers. Results presented show that reduced-order models can accurately predict time-marching solutions of aircraft for a wide range of motions, but with the advantage that reduced-order model predictions require on the order of a few seconds once the model is created. The results also demonstrate that the surrogate model being tested aids in reducing the overall computational efforts to develop reduced-order models.

The unsteady aerodynamic forces and moments acting on a fast-maneuvering fighter aircraft can have a significant effect on the aircraft's calculated stability and control characteristics. Some observed unsteady aerodynamic phenomena include aircraft buffeting, wing rock, roll reversal, and directional instability (Pamadi 2004). The aeroelastic instabilities of flutter or limit-cycle oscillations are also associated with unsteady aerodynamic loads (Wright and Cooper 2008). Despite great efforts using the best available predictive capabilities, nearly every major fighter program since 1960 has had costly issues with nonlinear aerodynamic or fluid–structure interactions that were not discovered until flight testing (Chambers and Hall 2004). Some recent aircraft that have experienced unexpected characteristics are the F/A-18, F-18E, and F-22 (Chambers and Hall 2004; Hall, Woodson, and Chambers 2005). The lack of a full understanding of unsteady aerodynamics typically leads to "cut and try" efforts, which result in very expensive and time-consuming solutions (Hall 2004). Current tools of computational fluid dynamics (CFD) have recently become credible for modeling unsteady nonlinear physics and hence would help to reduce the amount of wind-tunnel and flight testing required (Silva 1993). With advanced computing techniques, one straightforward way to calculate unsteady aerodynamics of a maneuvering aircraft is to develop a full-order mathematical model based on direct solution of the discretized Navier–Stokes equations coupled with the dynamic equations governing the aircraft's motion (Ghoreyshi, Jirásek, and Cummings 2011). A full-order model for stability-and-control analysis is a computationally very expensive approach, since such a model requires a large number of coupled computations for different values of motion frequency and amplitude. An alternative approach to solving the full-order model is to develop a reduced-order model (ROM) that seeks to approximate CFD results by extracting information from a limited number of full-order simulations. Ideally, the specified ROM can predict aircraft responses over a wide range of amplitudes

0.6. *12th AIAA Atmospheric Flight Mechanics Conference*. 19–21 August, Snowmass, CO. AIAA–85–1828.

Jones, D. R., M. Schonlau, and W. J. Welch. 1998. Efficient global optimization of expensive black-box functions. *Kluwer Academic Publications* 13: 455–492.

Leishman, J. G. 1993. Indicial lift approximations for two-dimensional subsonic flow as obtained from oscillatory measurements. *Journal of Aircraft* 30 (3): 340–351.

Leishman, J. G., and G. L. Crouse. 1989. *State-space model for unsteady airfoil behavior and dynamic stall. 30th AIAA/ASME/ASCE/AHS/ASC Structures, Structural Dynamics & Materials Conference,* 19–22 April 2004, Palm Springs, CA. AIAA Paper 89-1319.

Leishman, J. G., and K. Q. Nguyen. 1989. State-space representation of unsteady airfoil behavior. *AIAA Journal* 28 (5): 836–844.

Librescu, L., and O. Song. 2006. *Thin-walled composite beams: Theory and application*. Dordrecht, Netherlands: Springer.

Mackman, T. J., C. B. Allen, M. Ghoreyshi, and K. J. Badcock. 2011. *Comparison of adaptive sampling methods for generation of aerodynamic models for flight simulations. 49th AIAA Aerospace Meeting,* 4–7 January, Orlando, FL. AIAA Paper 2011–1171.

McCallen, R., F. Browand, and J. Ross. 2004 *The aerodynamics of heavy vehicles: Trucks, buses, and trains*. Berlin, Germany: Springer-Verlag.

Menter, F. 1994. Two-equation eddy-viscosity turbulence models for engineering applications. *AIAA Journal* 32 (8): 1598–1605.

Morton, S. A., R. M. Cummings, and D. B. Kholodar. 2004. *High resolution turbulence treatment of F/A-18 tail buffet. 45th AIAA/ASME/ASCE/AHS/ASC Structures, Structural Dynamics, and Materials Conference,* 19–22 April, Palm Springs, CA. AIAA Paper 2004-1676.

Morton, S. A., J. R. Forsythe, A. M. Mitchell, and D. Hajek. 2002. Detached-eddy simulations and Reynolds-averaged Navier-Stokes simulations of delta wing vortical flowfields. *Journal of Fluids Engineering* 124 (4): 924–932.

Pamadi, B. N. 2004. *Performance, stability, dynamics, and control of airplanes.* AIAA Education Series. Reston, VA: American Institute of Aeronautics and Astronautics.

Reisenthel, P. H. 1997. *Development of a nonlinear indicial model using response functions generated by a neural network. 35th AIAA Aerospace Science Meeting,* 6–9 January, Reno, NV. AIAA Paper 97–0337.

Reisenthel, P. H., and M. T. Bettencourt. 1999. *Data-based aerodynamic modeling using nonlinear indicial theory. 37th AIAA Aerospace Science Meeting,* 11–14 January, Reno, NV. AIAA Paper 97–0763.

Romero, D. A., C. Amon, S. Finger, and I. Verdinelli. 2004. Multi-stage Bayesian surrogates for the design of time-dependent system. In *Proceedings of ASME 2004 Design Engineering Technical Conference and Computers and Information in Engineering,* September 28–October 2, Salt Lake City, UT 405–414, DETC 2004-57510.

Schröder, W. 2010. *Summary of flow modulation and fluid-structure interaction findings*. Berlin, Germany: Springer-Verlag.

Silva, W. A. 1993. Application of nonlinear systems theory to transonic unsteady aerodynamics responses. *Journal of Aircraft* 30 (5): 660–668.

Singh, R., and J. Baeder. 1997. Direct calculation of three-dimensional indicial lift response using computational fluid dynamics. *Journal of Aircraft* 34 (4): 465–471.

Spalart, P. R., and S. R. Allmaras. 1992. *A one equation turbulence model for aerodynamic flows.* AIAA Paper 1992–0439. *30th AIAA Aerospace Science Meeting*, 6–9 January 1992, Reno, NV.

Spalart, P. R., and M. Schur. 1997. On the sensitisation of turbulence models to rotation and curvature. *Aerospace Science and Technology* 1 (5): 297–302.

Strang, W. Z., R. F. Tomaro, and M. J. Grismer. 1999. *The defining methods of Cobalt: A parallel, implicit, unstructured Euler/Navier-Stokes flow solver. 37th AIAA Aerospace Science Meeting,* 11–14. AIAA Paper 1999–0786.

Tobak, M., and G. T. Chapman. 1985. *Nonlinear problems in flight dynamics involving aerodynamic bifurcations.* NASA TN-86706. Moffet Field, CA: National Aeronautics and Space Administration.

Tobak, M., G. T. Chapman, and L. B. Schiff. 1984. *Mathematical modeling of the aerodynamic characteristics in flight dynamics.* NASA TN-85880. Moffet Field, CA: National Aeronautics and Space Administration.

Tomaro, R. F., W. Z. Strang, and L. N. Sankar. 1997. *An implicit algorithm for solving time dependent flows on unstructured grids. 35th AIAA Aerospace Science Meeting,* 6–9 January, Reno, NV. AIAA Paper 1997–0333.

Tyssel, L. 2000a. Hybrid grid generation for complex 3D geometries. In *Proceedings of the 7th International Conference on Numerical Grid Generation in Computational Field Simulation,* 25–28 September, Whistler, Canada, International Society of Grid Generation.

engineering from the University of Southern California in 1988. He was named professor of aeronautics at the U.S. Air Force Academy in 2004, where he is the Discipline Director for Aerodynamics and the research director for the Modeling & Simulation Research Center. Prior to serving at the Academy he was professor of aerospace engineering at Cal Poly from 1986 through 2004, where he served as department chair for four years. He worked for Hughes Aircraft Company in the Missile Systems Group as a missile aerodynamicist from 1979 through 1986. He completed a National Research Council postdoctoral research fellowship at NASA Ames Research Center in 1990, working on the computation of high angle-of-attack flowfields in the Applied Computational Fluids Branch. He was named an AIAA Associate Fellow in 1990, received the AIAA National Faculty Advisor Award in 1995, and is the past chairman of the AIAA Student Activities Committee. In addition, he has been awarded the USAF Science and Engineering Award, the Frank J. Seiler Research Award, the Boyer Award for Innovative Excellence in Teaching, Learning, and Technology, and the TRW Excellence in Teaching Award. He is currently a member of the AIAA Fluid Dynamics Technical Committee and the AIAA Student Activities Committee, and is co-author of the undergraduate textbook titled Aerodynamics for Engineers. He has published over 50 articles in peer-reviewed journals and over 120 technical meeting papers.

References

Balakrishna, S., and T. Niranjana. 1987. *Wind tunnel dynamic flying study of the pitching moment derivatives of the Standard Dynamics Model in active control. AIAA Atmospheric Flight Mechanics Conference,* 17–19 August 1987, Monterey CA. AIAA Paper 87-2626.

Beyers, M. E. 1983. Subsonic roll oscillation experiments on the Standard Dynamic Model. *AIAA Atmospheric Flight Mechanics Conference,* 15–17 August, Gatlinburg, TN. AIAA–83–2134.

Bisplinghoff, R. L., H. Ashley, and R. L. Halfman. 1996. *Aeroelasticity*. Mineola, N.Y.: Dover Publications.

Chambers, J. R., and R. M. Hall. 2004. Historical review of uncommanded lateral-directional motions at transonic conditions. *Journal of Aircraft* 41 (3): 436–447.

Cummings, R. M., S. A. Morton, and D. R. McDaniel. 2008. Experiences in accurately predicting time-dependent flows. *Progress in Aerospace Sciences* 44 (4): 241–257.

Da Ronch, A., D. Vallespin, M. Ghoreyshi, and K. J. Badcock. 2012. Evaluation of dynamic derivatives using computational fluid dynamics. *AIAA Journal* 50 (2): 470–484.

Forsythe, J. R., K. A. Hoffmann, R. M. Cummings, and K. D. Squires. 2002. Detached-eddy simulation with compressibility corrections applied to a supersonic axisymmetric base. *Journal of Fluids Engineering* 124 (4): 911–923.

Forsythe, R., K. D. Squires, K. E. Wurtzler, and P. R. Spalart. 2004. Detached-eddy simulation of fighter aircraft at high alpha. *Journal of Aircraft* 41 (2): 193–200.

Forsythe, J. R., and S. H. Woodson. 2005. Unsteady computations of abrupt wing stall using detached-eddy simulations. *Journal of Aircraft* 42 (3): 606–616.

Ghoreyshi, M., K. J. Badcock, and M. A. Woodgate. 2009. Accelerating the numerical generation of aerodynamic models for flight simulation. *Journal of Aircraft* 46 (3): 972–980.

Ghoreyshi, M., and R. M. Cummings. 2012. *Challenges in the aerodynamics modeling of an oscillating and translating airfoil at large incidence angles.* 50th AIAA Aerospace Meeting, 9–12 January 2012, Nashville, TN. AIAA Paper 2012-0690.

Ghoreyshi, M., A. Jirásek, and R. M. Cummings. 2011. *CFD modeling for trajectory predictions of a generic fighter configuration. AIAA Atmospheric Flight Mechanics Conference,* 19–21 August, Portland, OR. AIAA Paper 2011–6523.

Ghoreyshi, M., A. Jirásek, and R. M. Cummings. 2012. Computational investigation into the use of response functions for aerodynamic loads modeling. *AIAA Journal* 50 (6): 1314–1327.

Gottlieb, J. J., and C. P. T. Groth. 1998. Assessment of Riemann solvers for unsteady one-dimensional inviscid flows of perfect gasses. *Journal of Fluids and Structure* 78 (2): 437–458.

Hall, R. M. 2004. Overview of the Abrupt Wing Stall Program. *Progress in Aerospace Sciences* 40 (7): 417–452.

Hall, R. M., S. H. Woodson, and J. R. Chambers. 2005. Accomplishments of the Abrupt-Wing-Stall Program. *Journal of Aircraft* 42 (3): 653–660.

Huang, X. Z. 2000. *Wing and fin buffet on the Standard Dynamic Model.* RTO Technical Report RTO-TR-26. Quebec, Canada: The Research and Technology Organization (RTO) of NATO.

Jeans, T., D. McDaniel, R. M. Cummings, and W. Mason. 2009. Aerodynamic analysis of a generic fighter using delayed detached-eddy simulations. *Journal of Aircraft* 46 (4): 1326–1339.

Jermey, C., and L. B. Schiff. 1985. Wind tunnel investigation of the aerodynamic characteristics of the Standard Dynamics Model in coning motion at Mach

pitch-damping derivatives, but extraction of dynamic derivatives from harmonic motions results in the in-phase and out-of-phase components (Leishman 1993), requiring additional work to separate each derivative from these components.

ROM predictions

A ROM is now created along with a time-dependent surrogate model to determine the terms in Equations 1 and 2 at each time step. The validity of the ROM is tested for several arbitrary pitching and plunging motions. These motions start from different steady-state conditions (not being used at sample design) and run for different amplitudes and frequencies. Note that the plunge motions have no rotation, but the angle of attack changes due to the vertical displacements of the grid; this angle is named the effective angle of attack, denoted by α_e:

$$\alpha_e = \tan^{-1}\left(\frac{\dot{h}}{V}\right), \tag{18}$$

where $\dot{h}$ shows the vertical displacement of the grid and V is the free-stream velocity. The maximum effective angle of attack for a plunge starting at a zero-degree angle of attack is determined by the Strouhal number, St $= 2fH/V$, such that $\alpha_e^{\max} = \tan^{-1}(\pi \mathrm{St})$, where f is the frequency and H is the plunge amplitude. The ROM predictions are compared with time-accurate CFD simulations in *Figures 10 and 11*. The time-accurate solutions are labeled as "CFD" in the plots. *Figures 10 and 11* show that the ROM lift and pitch moment predictions agree well with the full-order CFD simulation values. Small discrepancies are found in the pitch moment predictions at negative angles of attack. This is likely due to the fact that SDM pitch moment is not symmetric with angle of attack, and hence the response functions generated at positive angles cannot predict the slope changes correctly. Note that the average cost of generating each full-order simulation is around 1,280 CPU hours, while the ROM predictions require on the order of a few seconds.

Conclusions

The use of indicial functions for unsteady- and nonlinear-aerodynamics modeling of a generic fighter configuration was investigated in this article. Only the longitudinal aerodynamic forces and moments were considered; thus, the aircraft responses corresponding to a step change in angle of attack and pitch rate were found. The step functions were calculated using a CFD and grid-motion approach for a set of samples defined in the space of angle of attack and Mach number. The results show that indicial functions have a peak response at initial time steps. This is related to a traveling acoustic wave formed by the flow disturbance. At higher Mach numbers, the peak values are diminished due to compressibility. A time-dependent surrogate model was used to interpolate these functions for the new conditions. The ROMs were tested by comparison of the model output with time-accurate CFD simulations for several motions. The results show that predictions agree well with full-order CFD simulation values. Future work will extend this study to include samples generated by Latin hypercube sampling and generate ROMs for maneuvers with six degrees of freedom. ❑

MEHDI GHOREYSHI received his M.Sc. and Ph.D. in gas turbine engineering from Cranfield University, UK, before he joined the University of Liverpool as a research associate in November 2006. At Liverpool, his research interest was generation of aerodynamic models for flight dynamic analysis. Mehdi was awarded a Resident Research Associateship by National Research Council in August 2010 and moved to the US Air Force Academy at the same time. He is currently working on the reduced order modeling of nonlinear and unsteady aerodynamics.

DR. MARTIQUA L POST graduated in 1999 from Union College in Schenectady, New York with a B.S. in mechanical engineering. She earned a MS in mechanical engineering from the University of Notre Dame in Indiana in August 2001 and earned a Ph.D. in aerospace and mechanical engineering from the University of Notre Dame in May 2004. She is an associate professor in the Department of Aeronautics at the United States Air Force Academy, Colorado Springs CO. She started at the Academy in July 2005. Dr. Post specializes in Fluid Dynamics and has taught over eight different college courses at USAFA and Notre Dame. She has taught subjects ranging from Computational Fluid Dynamics to Aerothermodynamics. Her experimental research interests include flow control, where she has a patent on plasma actuator technology. Her computation research interests are focused on modeling unsteady aerodynamics of fighter aircraft configurations by mathematical modeling of reduced-order unsteady aerodynamic models, generation of CFD training maneuvers, and numerical simulations. Dr. Post is the Chair-Elect of the Applied Aerodynamics Technical Committee and a member of the Student Activities Committee for the American Institute of Aeronautics and Astronautics.

DR. RUSSELL M. CUMMINGS graduated from California Polytechnic State University with a B.S. and M.S. in Aeronautical Engineering in 1977 and 1985, respectively, before receiving his Ph.D. in aerospace

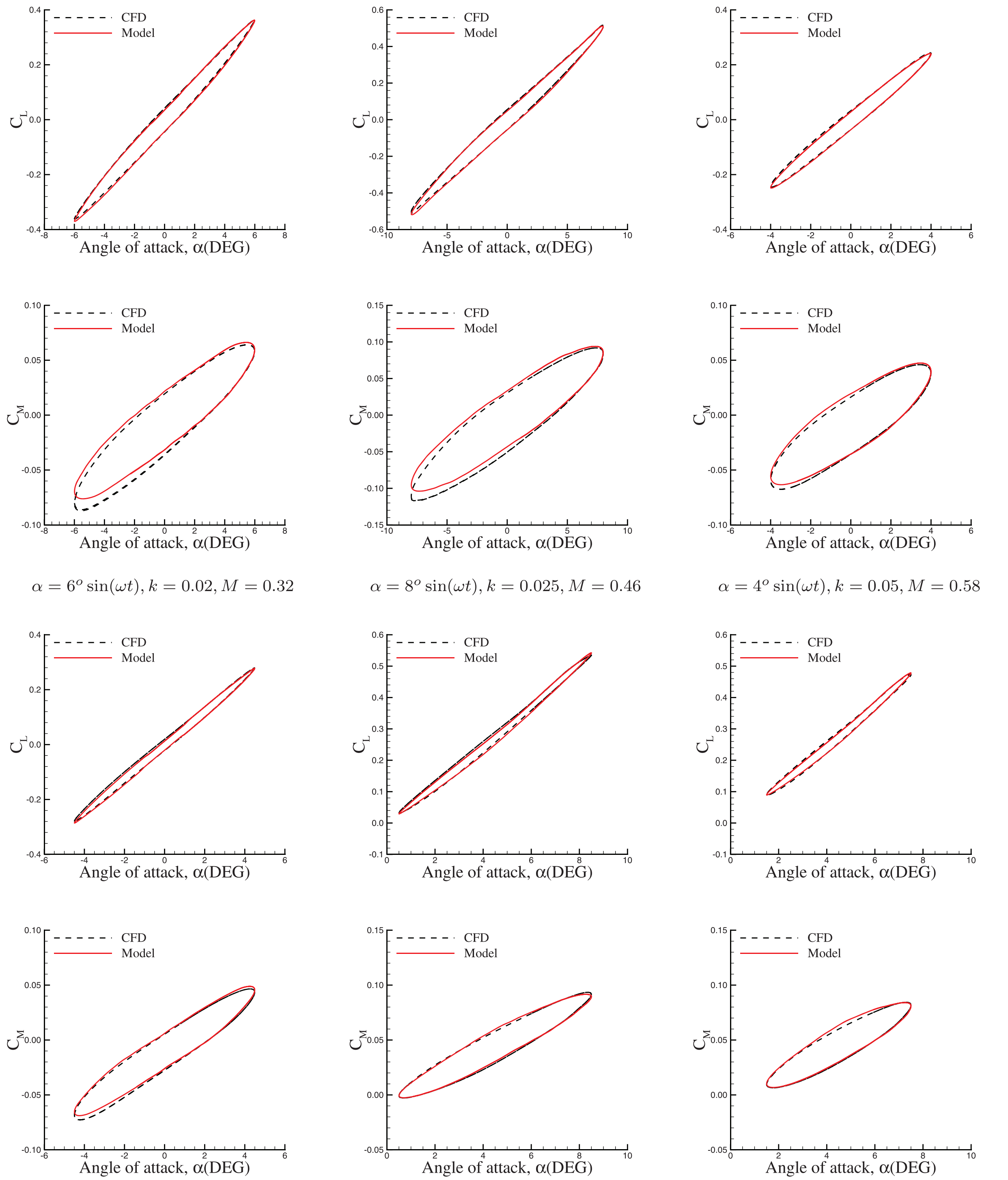

$\alpha = 6^o \sin(\omega t), k = 0.02, M = 0.32$ $\alpha = 8^o \sin(\omega t), k = 0.025, M = 0.46$ $\alpha = 4^o \sin(\omega t), k = 0.05, M = 0.58$

$\alpha = 4.5^o \sin(\omega t), k = 0.015, M = 0.66$ $\alpha = 4.5^o + 4^o \sin(\omega t), k = 0.02, M = 0.37$ $\alpha = 4.5^o + 3^o \sin(\omega t), k = 0.035, M = 0.46$

Figure 11. ROM prediction of pitching motions.

the experimental pitch moment data, although the CFD data do not include the effects of rate of change of angle of attack, i.e., $C_{m\dot{\alpha}}$. Typically, C_{mq} is the largest factor in the sum $C_{mq} + C_{m\dot{\alpha}}$, typically accounting for 90 percent of the sum. Again, the underestimation of experimental data is likely due to different inlet geometries in the wind-tunnel and the SDM geometry used. Note that the indicial-function approach allows the direct calculation of

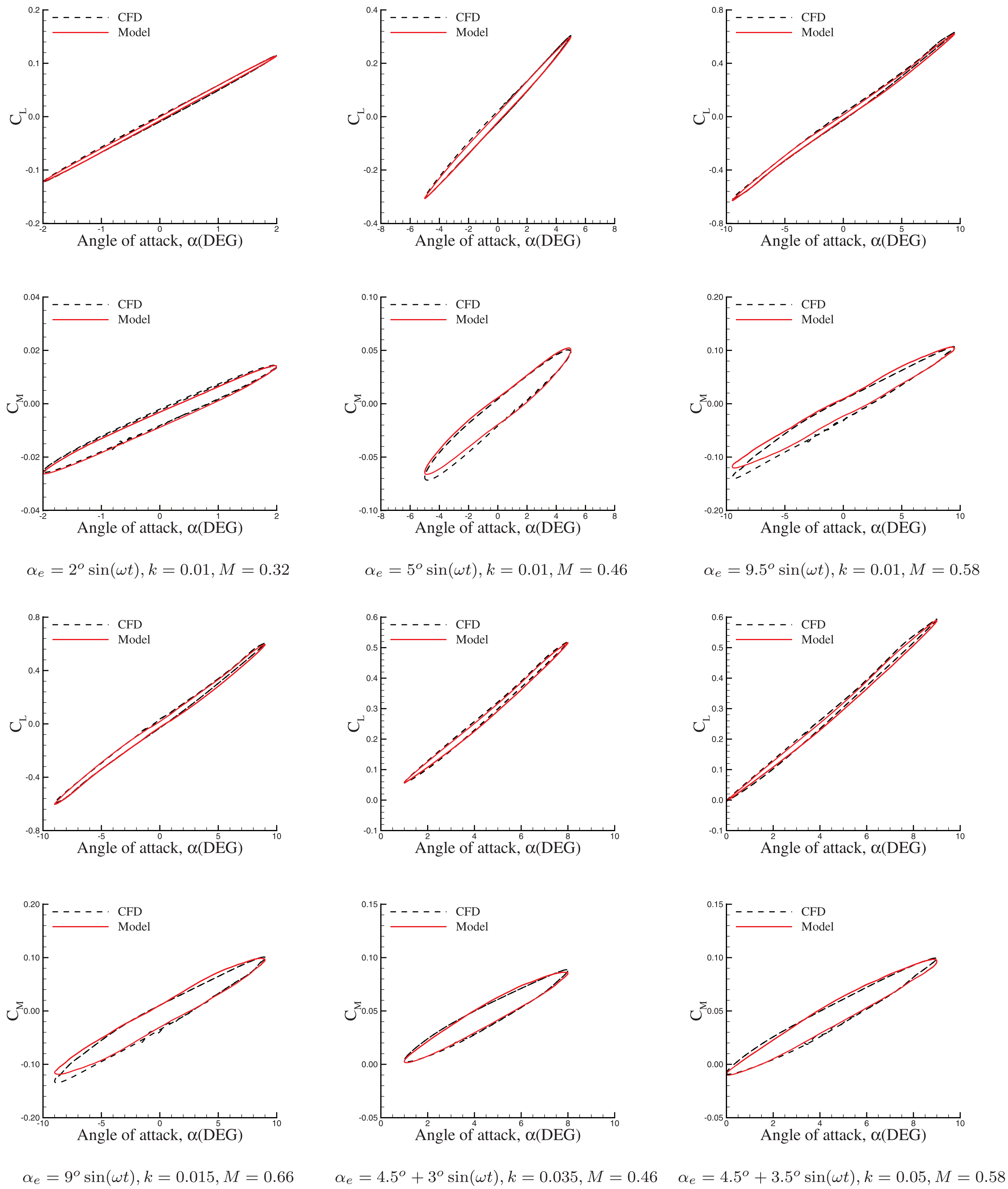

Figure 10. ROM prediction of plunging motions. In above ω is angular velocity and k is reduced frequency.

moment have initial peaks due to the initial perturbations and asymptotically reach the steady-state value. *Figure 8* shows that increasing Mach numbers result in the increase of steady-state C_{Lq} and the decrease of steady-state C_{mq} (the so-called pitch-damping derivative). *Figure 9* compares the steady-state C_{mq} values calculated from the CFD code with the out-of-phase components of pitch moment derivative—i.e., $C_{mq} + C_{m\dot{\alpha}}$—measured at different Mach numbers and zero angle of attack; these experimental data are detailed by Da Ronch et al. (2012). Like the static predictions, the CFD values slightly underestimate

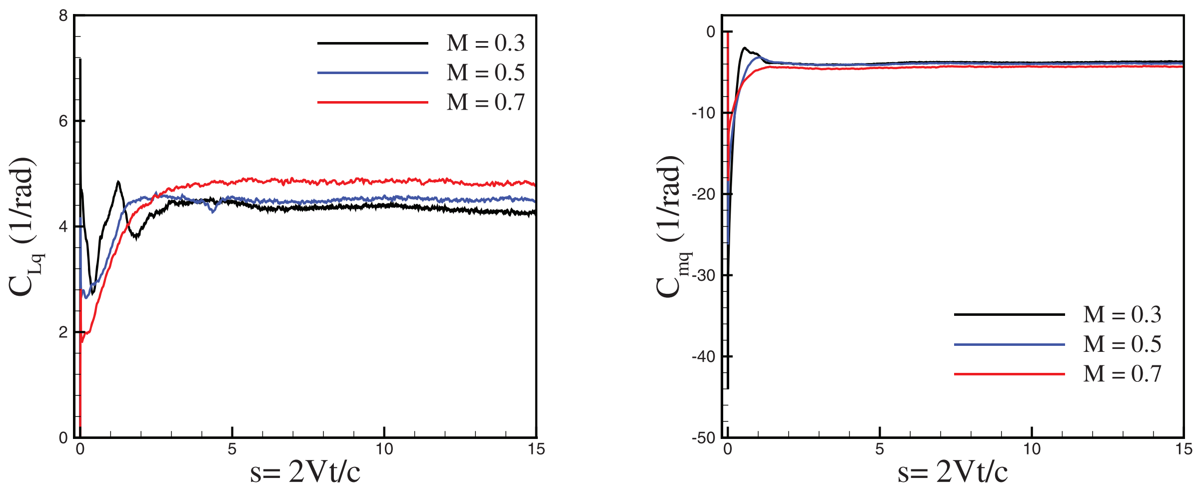

(a) Pitch rate lift indicial functions (b) Pitch rate pitch moment indicial functions

Figure 8. Lift and pitch moment indicial solutions due to pitch rate for $\alpha = 0^{\circ}$. The pitch axis and moment reference point are located at 35 percent Mean Aerodynamic Center (MAC).

using factorial design; these points are shown in *Figure 6*. The indicial functions are calculated using the CFD and grid-motion approach for each sample condition. All these calculations started from a steady-state solution such that the Mach number in the steady-state simulations corresponds to each sample Mach number. For the indicial functions due to angle of attack, the steady-state angle of attack is set to zero degrees, but for the indicial functions due to pitch rate, the steady angle of attack corresponds to each sample α. The step-function calculations are second order in time with a nondimensional time step of $\Delta t^{*} = \Delta t.V/c = 0.01$. For more details on time-step selection, the reader is referred to the work of Cummings, Morton, and McDaniel (2008).

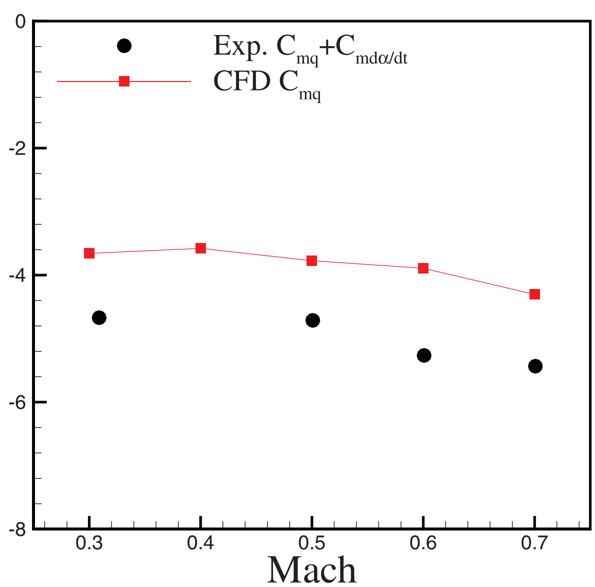

Figure 9. Validation of C_{mq} values calculated from pitch-rate indicial functions. Experimental data are from Da Ronch et al. (2012).

The calculated indicial functions due to angle of attack are shown in *Figure 7* for $M = 0.3$ and $M = 0.6$. *Figures 7(a)* and *7(b)* show that the indicial lift has a peak at $s = 0$ followed by a rapidly falling trend. The lift again builds up and asymptotically reaches the steady-state value. The pitch moment has a negative peak at $s = 0$, as shown in *Figures 7(c)* and *7(d)*. The initial peak can be explained based on the energy of acoustic-wave systems created by the initial perturbation (Ghoreyshi and Cummings 2012). The most obvious difference between responses at low and high speeds is that the initial peak becomes smaller for higher speeds. An explanation is given by Leishman (1993): this is due to the propagation of pressure disturbances at the speed of sound, as compared with the incompressible case, where the disturbances propagate at infinite speed. *Figure 7* also shows that the initial values of the indicial functions are invariant with angle of attack, but the intermediate trend and steady-state values change depending on the angle of attack. Although the final values of indicial lift are nearly unchanged for angles of attack below five degrees, the pitch moment's final values are different even at small angles of attack, due to vortices on the wing.

The effects of Mach number on the lift and pitch moment indicial functions are shown in *Figure 8*. As with angle-of-attack response, the lift and pitch

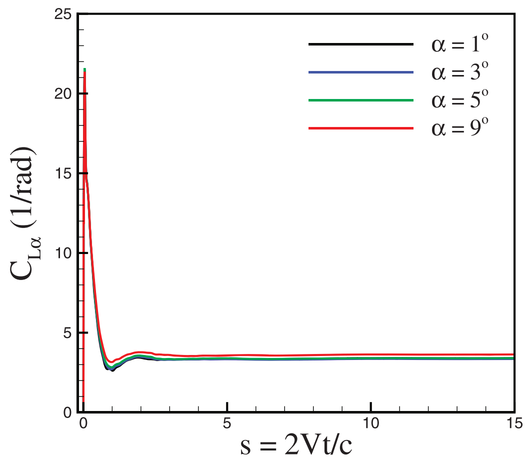

(a) Nonlinear lift responses at $M = 0.3$

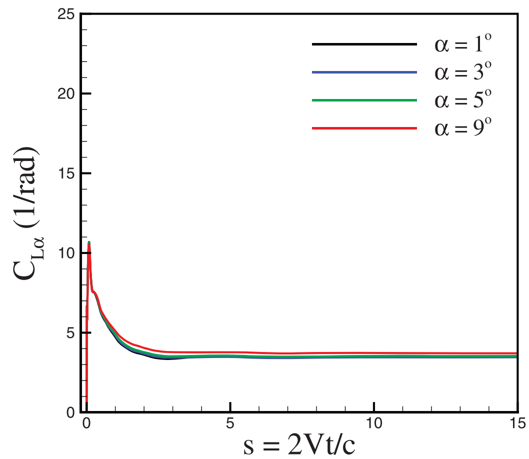

(b) Nonlinear lift responses at $M = 0.6$

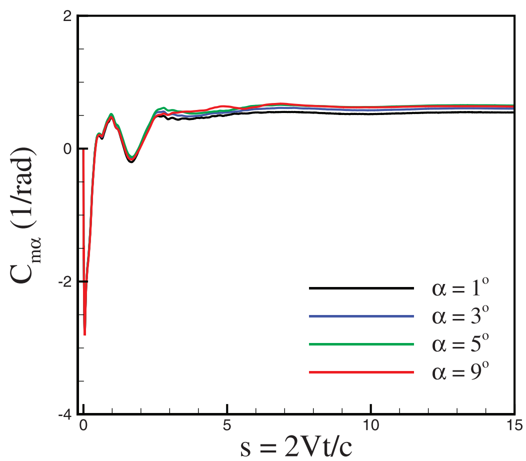

(c) Nonlinear pitch moment responses at $M = 0.3$

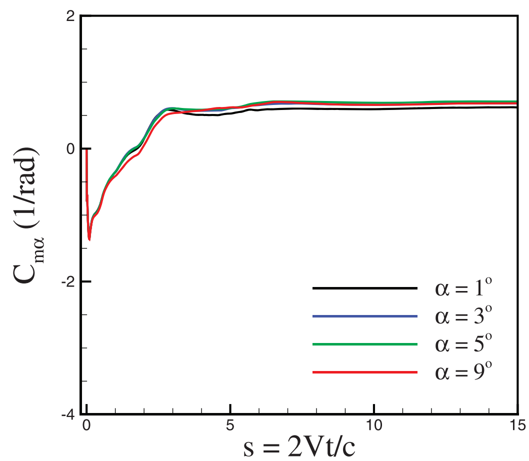

(d) Nonlinear pitch moment responses at $M = 0.6$

Figure 7. Nonlinear lift and pitch moment indicial solutions due to angle of attack for M = 0.3 and 0.6.

other toward the trailing edge of the wing, as shown in *Figure 5(c)*. With a slight increase in angle of attack, the wing vortex appears to break down quickly, as shown in *Figure 5(d)*. The vortex breakdown leads to a smaller rate of increase in lift and a negative pitch moment slope.

The vortex-breakdown phenomenon is asymmetric, and hence the lateral force and moment coefficients suddenly start to change very fast. At 22 degrees, the strake vortex is also burst, as shown in *Figure 5(e)*. Finally, at 25 degrees there is no sign of a wing vortex, as shown in *Figure 5(f)*.

Calculation of indicial functions

The indicial response functions in this article are interpolated from some available samples in the space of angle of attack and free-stream Mach number. Note that these functions only need to have dependency on angle of attack and Mach number, and once they have been calculated they can be used to predict the aerodynamic response to any frequency of interest. The samples could be generated using methods of factorial designs, Latin hypercube sampling, low-discrepancy sequences, or designs based on statistical optimality criteria (A-, D- and G-optimal designs; Mackman et al 2011). Factorial designs are extremely simple to construct and have been used in this work. The considered SDM motions encompass α and M values in the ranges of $[-10^\circ, 10^\circ]$ and $[0.3, 0.7]$, respectively. Assuming symmetrical flow solutions with respect to the angle of attack, the indicial functions are only calculated for positive angles of attack. A set of samples including 50 points is defined on the α and M space

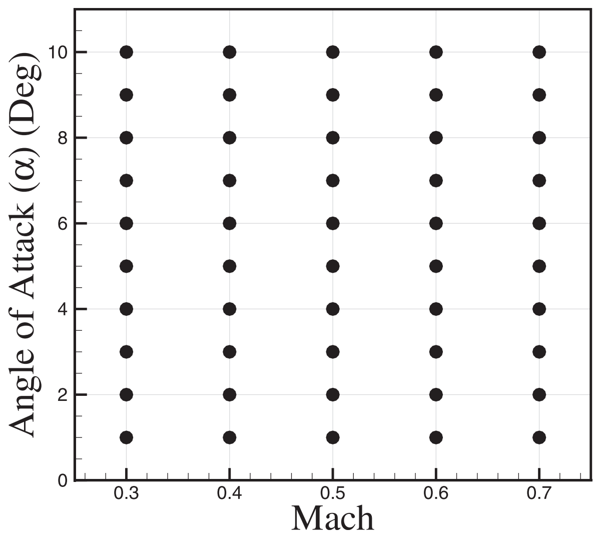

Figure 6. Design samples.

movement of vortex breakdown has significant effects on the pitching moment. Validation of CFD codes for predicting these effects can be a very challenging task.

In this article, only unsteady RANS calculations are used. A full-span geometry mesh is available, shown in *Figure 3*. The mesh was generated in two steps. In the first step, the inviscid tetrahedral mesh was generated using the ICEM CFD code. This mesh was then used as a background mesh by TRITET (Tyssel 2000a, 2000b), which builds prism layers using a frontal technique. TRITET rebuilds the inviscid mesh while respecting the size of the original inviscid mesh from ICEM CFD. The full-span geometry mesh consists of a nine-million-point mesh and 19.5 million cells.

Results

Static predictions

Wind-tunnel experiments (Huang 2000) were first used to validate the CFD predictions at low speed. The conditions of the tests were $V = 110$ m/s, Re = 0.57 million (Re=Reynolds number), and $\beta = 5^\circ$ for $\alpha = 0$ to 90°. All CFD simulations were run at free-stream conditions consistent with flow conditions in wind-tunnel tests. For the flow solution, RANS equations are discretized by second-order spatial and temporal operators. The turbulence models used are Spalart–Allmaras (Spalart and Allmaras 1992), Spalart–Allmaras with rotation/curvature correction (SARC; Spalart and Schur 1997), and Menter's (1994) shear stress transport (SST). The relatively low-cost Spalart–Allmaras model is the most popular one-equation turbulence model for flows with an attached boundary layer (McCallen, Browand, and Ross 2004), but the model has a large viscosity in the core of vortices that results in diffusion of the vortex structure (Schröder 2010). On the other hand, the SARC model provides a lower eddy viscosity for vortical flow predictions (Schröder 2010). The SST model is a hybrid $k - \varepsilon$ and $k - \omega$ turbulence model (Morton, Cummings, and Kholodar 2004). Typical $\varepsilon - \omega$ models are well behaved in the near-wall region, where low-Reynolds-number corrections are not required. However, they are generally sensitive to the free-stream values of ω. On the other hand, $k - \varepsilon$ models are relatively insensitive to free-stream values, but behave poorly in the near-wall region. The SST model uses a parameter F_1 to switch from $k - \omega$ to $k - \varepsilon$ in the wake region to prevent the model from being sensitive to free-stream conditions (Morton, Cummings, and Kholodar 2004).

All simulations were computed on an unstructured mesh with prisms in the boundary layer and tetrahedra elsewhere on full-span geometry. The cases were run on the Cray XE6 and Cray XE6 (open system) machines at the Engineering Research Development Center (Garnet, with 2.7 GHz core speed, and Chugach, with 2.3GHz core speed), which have approximately 20,000 and 11,000 cores, respectively. The total run times of 1,000 iterations using 128 processors for the SARC and SST turbulence models were 5 and 6 hours, respectively. The static force and moment coefficients are compared with experiments in *Figure 4*.

The comparisons show that there is a good agreement between RANS predictions and the measurements for angles of attack below 25 degrees. However, all turbulence models predict a positive pitch moment slope at zero degrees, while experiments show a falling trend at this angle. This is likely due to different inlet geometries in wind-tunnel and free-flight models. At five degrees, a pair of vortices emanating from strake and wing leading edge have formed, as shown in *Figure 5(a)*. These vortices do not exhibit breakdown and do not interact over the airframe. The vortex formation causes additional increase of lift and pitch moment coefficients. In experimental tests, the sign of pitch moment is reversed at this angle, while CFD shows a jump in the moment rate of increase. No significant changes in lateral force and moment coefficients were observed at this angle.

The vortices grow in size and strength with increasing angle of attack. At 10 degrees, the center of a vortex of the wing is shifted laterally while the shedding point is moved forward, as shown in *Figure 5(b)*. There are still no signs of vortex breakdown. The lateral moments slightly change due to the movement of the wing vortex. Around 14 degrees, the two vortices wind around each

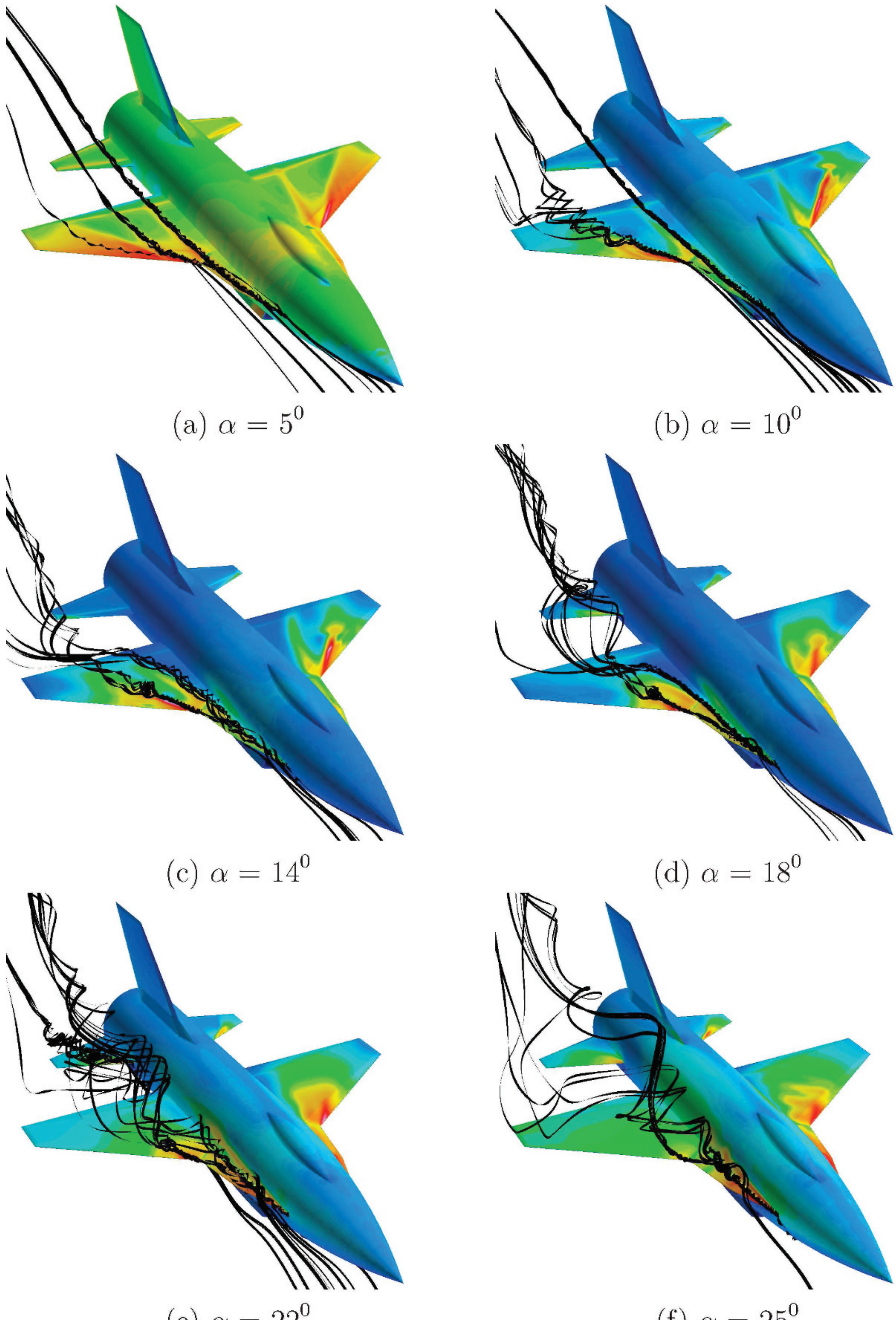

(a) $\alpha = 5^0$ (b) $\alpha = 10^0$

(c) $\alpha = 14^0$ (d) $\alpha = 18^0$

(e) $\alpha = 22^0$ (f) $\alpha = 25^0$

Figure 5. SDM flow-field visualization. The calculations are for a Mach number of 0.3 and $\beta = 5$ using the SARC turbulence model.

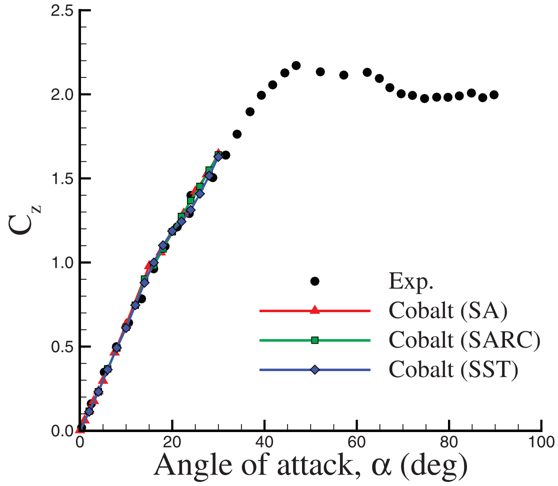

(a) normal force coefficient

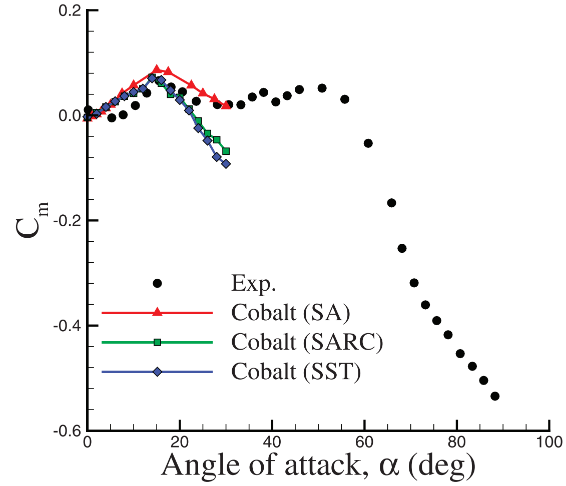

(b) pitch moment coefficient

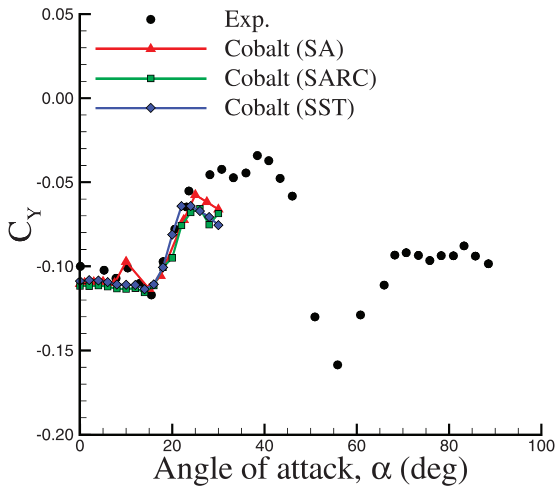

(c) side-force coefficient

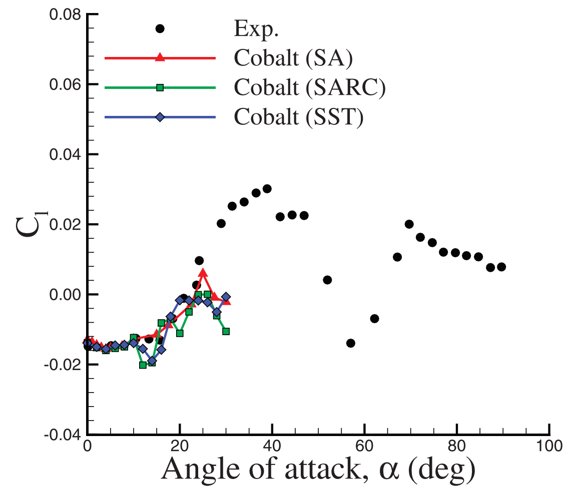

d) roll moment coefficient

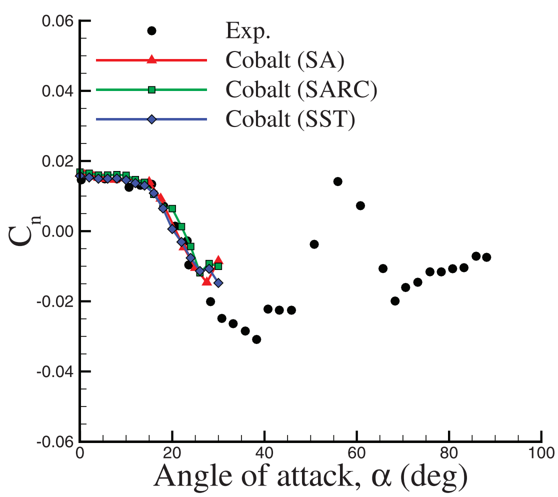

(e) yaw moment coefficient

Figure 4. Static aerodynamic predictions at V_0 = 100 m/s and β = β is side-slip angle.

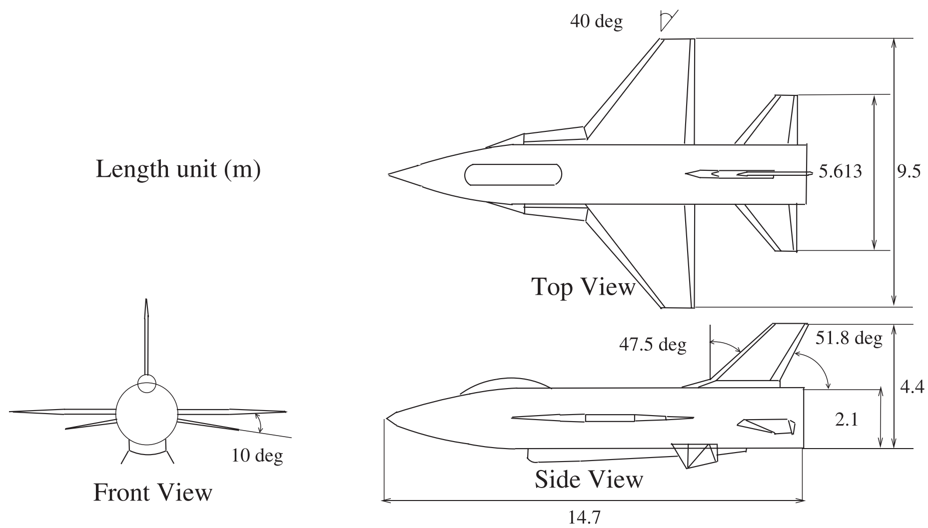

Figure 2. Standard Dynamic Model (SDM) layout (Huang 2000).

(1998). Next the vector of $\mathbf{R}(m \times 1)$ is defined from correlations between the new design parameter $\mathbf{x}_0$ and the m sample points, based on the distance formula in Equation 12:

$$\mathbf{r} = \begin{bmatrix} \exp\left[-\dfrac{d(\mathbf{x}_1,\mathbf{x}_0)}{\sigma^2}\right] \\ \exp\left[-\dfrac{d(\mathbf{x}_2,\mathbf{x}_0)}{\sigma^2}\right] \\ \vdots \\ \exp\left[-\dfrac{d(\mathbf{x}_m,\mathbf{x}_0)}{\sigma^2}\right] \end{bmatrix}. \tag{14}$$

Now $\widetilde{\mathbf{Z}}_i(\mathbf{x}_0)$ can be estimated as

$$\widetilde{\mathbf{Z}}_i(\mathbf{x}_0) = \sum_{j=0}^{n} \beta_{ij}\mathbf{f}_j(\mathbf{x}_0) + \mathbf{r}^T\mathbf{R}^{-1}[\mathbf{Z}_i(\mathbf{D}) - \mathbf{F}\beta], \tag{15}$$

where β is the n + 1–dimensional vector of regression coefficients; $\mathbf{Z}_i(\mathbf{D})$ is the observed responses at time step i = 1, 2, . . . , p; and matrix $\mathbf{F}$ is

$$\mathbf{F} = \begin{bmatrix} \mathbf{f}_0(x_1) & \mathbf{f}_1(x_1) & \cdots & \mathbf{f}_\mathbf{n}(x_1) \\ \vdots & \vdots & \ddots & \vdots \\ \mathbf{f}_0(x_m) & \mathbf{f}_1(x_m) & \cdots & \mathbf{f}_\mathbf{n}(x_m) \end{bmatrix}. \tag{16}$$

The total response at $\mathbf{x}_0$ is then a combination of the predicted values of each surrogate model:

$$\tilde{\mathbf{Z}}(\mathbf{x}_0) = \left[\tilde{\mathbf{Z}}_1(\mathbf{x}_0), \tilde{\mathbf{Z}}_2(\mathbf{x}_0), \ldots, \tilde{\mathbf{Z}}_p(\mathbf{x}_0)\right]. \tag{17}$$

Test case

The Standard Dynamics Model (SDM) is a generic fighter configuration based on the F-16 platform. The model includes a slender strake-delta wing, horizontal and vertical stabilizers, ventral fins, and a blocked-off inlet section. The three-view drawing is shown in *Figure 2*. This geometry has been tested extensively at various wind-tunnel facilities to collect wind-tunnel data (Balakrishna and Niranjana 1987; Beyers 1984; Jermey and Schiff 1985). Note that slightly different geometries were used in previous studies.

The lifting surfaces (strake, wing, and tail) have a thin airfoil with sharp leading edges. This enforces a fixed separation point in the leading edge and the formation of vortices over the surface. The vortex-induced suction pressure accounts for the additional lift, named vortex lift, which helps to delay stalling. The complex interaction of strake and wing vortices creates very nonlinear aerodynamic characteristics. Also, at high angles of attack, these vortices break down and cause a sudden reduction in lift. The forward

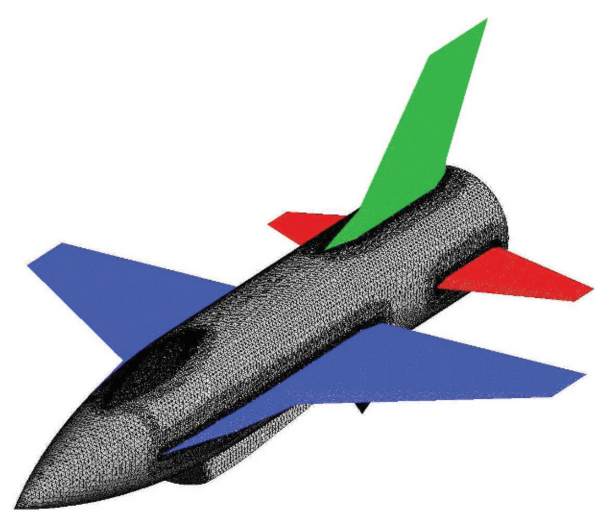

Figure 3. The SDM aircraft-surface mesh model.

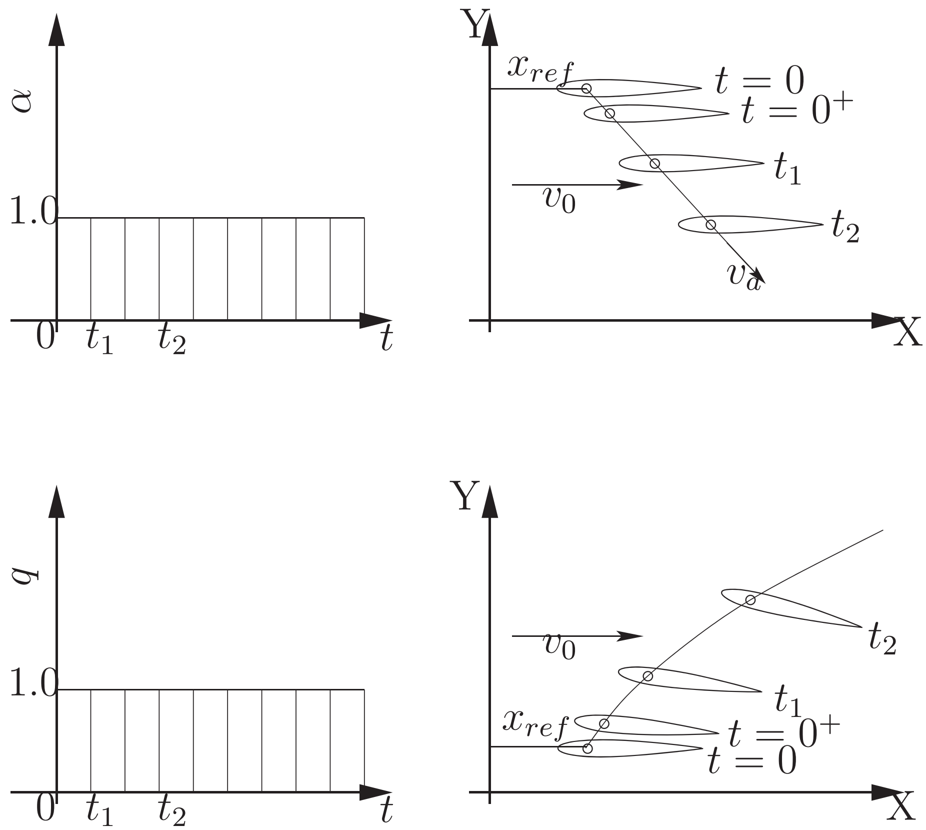

Figure 1. The grid motion for modeling a step change in angle of attack and pitch rate.

construct this surrogate model, the responses at each time step are assumed as a separate set, such that each column of the output matrix is a partial realization of the total response. In this sense, p surrogate models are created; they are denoted as $\mathbf{Z}_i(\mathbf{D})$ for $i = 1, 2, \ldots, p$. A universal-type kriging function (Ghoreyshi, Badcock, and Woodgate 2009) is used to approximate these models. Each $\mathbf{Z}_i(\mathbf{D})$ function can be approximated as the sum of a deterministic mean (trend) μ and a zero-mean spatial random process of ε with a given covariance structure of σ^2; therefore each function value at the new sample of $\mathbf{x}_0$ is

$$\tilde{\mathbf{Z}}_i(\mathbf{x}_0) = \mu + \epsilon, \tag{10}$$

where the tilde shows that the surrogate model is an approximation of the actual function. Universal kriging, which is used in this article, assumes that the mean value μ is a linear combination of known regression functions of $\mathbf{f}_0(x)$, $\mathbf{f}_1(x)$, . . . , $\mathbf{f}_n(x)$. In this article, the linear functions are used; therefore, $\mathbf{f}_0(x) = 1$ and $\mathbf{f}_j(x) = x_j$ for $j = 1, 2, \ldots, n$. This changes Equation 10 to

$$\tilde{\mathbf{Z}}_i(\mathbf{x}_0) = \sum_{j=0}^{n} \beta_{ij} \mathbf{f}_j(\mathbf{x}_0) + \epsilon, \tag{11}$$

where β_{ij} represent the regression coefficient for the jth regression function of the response function at time step $i = 1, 2, \ldots, p$. To estimate the spatial random process of ε, a spatially weighted distance formula is defined between samples given in matrix $\mathbf{D}$ such that for sample $\mathbf{x}_i$ and $\mathbf{x}_j$, the distance is written as

$$d(\mathbf{x}_i, \mathbf{x}_j) = \sum_{h=1}^{n} \theta_h \left| x_h^{(i)} - x_h^{(j)} \right|^{p_h}, \tag{12}$$

where the vertical bars indicate the Euclidean distance, the parameter $\theta_h \geq 0$ expresses the importance of the hth component of the input vector, and the exponent p_h ($\in [0, 1]$) is related to the smoothness of the function in the coordinate direction h. A correlation matrix $\mathbf{R}(m \times m)$ with a Gaussian spatial random process is then defined as

$$\mathbf{R} = \begin{bmatrix} \exp\left[-\frac{d(\mathbf{x}_1,\mathbf{x}_1)}{\sigma^2}\right] & \exp\left[-\frac{d(\mathbf{x}_1,\mathbf{x}_2)}{\sigma^2}\right] & \cdots & \exp\left[-\frac{d(\mathbf{x}_1,\mathbf{x}_m)}{\sigma^2}\right] \\ \vdots & \vdots & \ddots & \vdots \\ \exp\left[-\frac{d(\mathbf{x}_m,\mathbf{x}_1)}{\sigma^2}\right] & \exp\left[-\frac{d(\mathbf{x}_m,\mathbf{x}_2)}{\sigma^2}\right] & \cdots & \exp\left[-\frac{d(\mathbf{x}_m,\mathbf{x}_m)}{\sigma^2}\right] \end{bmatrix}. \tag{13}$$

To compute the kriging model, values must be estimated for β_{ij}, α, θ_h, and p_h. These parameters can be quantified using the maximum-likelihood estimator, as described by Jones, Schonlau, and Welch factorization. To accelerate the convergence solution of the discretized system, a point-implicit method using analytic first-order inviscid and viscous Jacobians is used. A Newtonian subiteration method is used to improve the time accuracy of the point-implicit method. Tomaro, Strang, and Sankar (1997) converted the code from explicit to implicit, enabling Courant–Friedrichs–Lewy numbers as high as 10^6. The Cobalt solver has been used at the Air Force Seek Eagle Office and the United States Air Force Academy for a variety of unsteady nonlinear aerodynamic problems of maneuvering aircraft (Forsythe, Hoffmann, et al. 2002; Forsythe, Squires, et al. 2004; Forsythe and Woodson 2005; Jeans et al. 2009; Morton et al. 2002).

CFD calculation of indicial functions

In this article, the indicial functions are directly calculated from Unsteady Reynolds-Averaged Navier Stokes (URANS) simulations using a grid-motion tool. Cobalt, the flow solver used, uses an arbitrary Lagrangian–Eulerian formulation and hence allows all translational and rotational degrees of freedom (Ghoreyshi, Jirásek, and Cummings 2012). The code can simulate both free and specified motions with six degrees of freedom. The rigid motion is specified from a motion input file. For the rigid motion, the location of a reference point on the aircraft is specified at each time step. In addition, the rotation of the aircraft about this reference point is also defined using the rotation angles of yaw, pitch, and roll (bank). The aircraft reference-point velocity V_a in an inertial frame is then calculated to achieve the required angles of attack and sideslip, and the forward speed. The velocity is then used to calculate the location. The initial aircraft velocity V_0 is specified in terms of Mach number, angle of attack, and sideslip angle in the main file. The instantaneous aircraft location for the motion file is then defined from the relative velocity vector V_a–V_0. For CFD-type calculation of a step change in angle of attack, the grid immediately starts to move at $t = 0$ to the right and downward, as shown in *Figure 1*. The translation continues over time with a constant velocity vector. Since there is no rotation, all the effects on aerodynamic loads are from changes in the angle of attack. For a unit step change in pitch rate, the grid moves and rotates simultaneously. The grid starts to rotate with a unit pitch rate at $t = 0$. To hold the angle of attack at zero during the rotation, the grid moves right and upward in *Figure 1*. All indicial function computations started from a steady-state solution and then advanced in time using second-order accuracy with five Newton subiterations. The steady-state solutions correspond to a zero-degree angle of attack and sideslip for the Mach number of interest.

Surrogate-based modeling of indicial functions

Having an ROM to predict the aerodynamic responses to any arbitrary motion over a wide flight regime could become a very expensive approach, because a large number of indicial functions need to be computed. In order to achieve a reasonable computational cost, a special time-dependent surrogate-based modeling approach is adapted to predict indicial responses for a new point from available (observed) responses. These observed responses are viewed as a set of time-correlated spatial processes where the output is considered a time-dependent function. Romero et al. (2004) have developed a framework for multistage Bayesian surrogate models for the design of time-dependent systems and tested their model for free vibrations of a mass-spring-damper system assuming the input parameters of stiffness and damping factor at different initial conditions. This framework is examined for reduced-order modeling of nonlinear and unsteady aerodynamic loads. Assume an input vector of $\mathbf{x}(t) = [x_1(t), x_2(t), \ldots, x_n(t)]$, where n represents the dimensionality of the input vector. To construct a surrogate model for fitting the input–output relationship, the unsteady aerodynamic responses corresponding to a limited number of input parameters (training parameters or samples) need to be generated. Design-of-experiment methods, for example, can be used to select m samples from the input space. The input matrix $\mathbf{D}(m \times n)$ is then defined as

$$\mathbf{D} = \begin{bmatrix} x_{11} & x_{12} & \cdots & x_{1n} \\ x_{21} & x_{22} & \cdots & x_{2n} \\ \vdots & \vdots & \ddots & \vdots \\ x_{m1} & x_{m2} & \cdots & x_{mn} \end{bmatrix}, \tag{8}$$

where rows correspond to different combinations of the design parameters. For each row in the input matrix, a time-dependent response was calculated at p discrete values of time; this information is summarized in the output matrix of $\mathbf{Z}(m \times p)$ as

$$\mathbf{Z} = \begin{bmatrix} y_{11} & y_{12} & \cdots & y_{1p} \\ y_{21} & y_{22} & \cdots & y_{2p} \\ \vdots & \vdots & \ddots & \vdots \\ y_{m1} & y_{m2} & \cdots & y_{mp} \end{bmatrix}, \tag{9}$$

where for modeling of aerodynamic loads, p equals the number of iterations used in time-marching CFD calculations. The objective of surrogate modeling is to develop a model that allows prediction of the aerodynamic response of $\mathbf{y}(\mathbf{x}_0) = (y_{01}, y_{02}, \ldots, y_{0p})$ at a new combination of input parameters $\mathbf{x}_0$. To

The unsteady-lift coefficient at time t is obtained by

$$C_L(t) = C_{L_0}(M) + \frac{d}{dt}\left[\int_0^t C_{L_\alpha}(t-\tau,\ \alpha,\ M)\alpha(\tau)d\tau\right] + \frac{d}{dt}\left[\int_0^t C_{Lq}(t-\tau,\ \alpha,\ M)q(\tau)d\tau\right], \tag{1}$$

where C_{L_0} denotes the zero-angle-of-attack lift coefficient (found from static calculations) and M denotes the free-stream Mach number. Note that the indicial response function with respect to the rate of change of velocity—i.e., $\dot{V}$—is assumed to be small and is not modeled. Likewise, the time responses in pitch moment due to the step changes in α and q are denoted as $C_{m\alpha}$ and C_{mq}, and the pitch moment is estimated as follows:

$$C_m(t) = C_{m0}(M) + \frac{d}{dt}\left[\int_0^t C_{m\alpha}(t-\tau,\ \alpha,\ M)\alpha(\tau)d\tau\right] + \frac{d}{dt}\left[\int_0^t C_{mq}(t-\tau,\ \alpha,\ M)q(\tau)d\tau\right]. \tag{2}$$

The unsteady effects in drag force are assumed to be small and therefore are not discussed here. The response function due to pitch rate—i.e., $C_{jq}(\alpha, M)$ for $j = L, m$—can be estimated using a time-dependent interpolation scheme from the observed responses. This value is next used to estimate the second integrals in Equations 1 and 2; however, the estimation of the integral with respect to the angle of attack needs more explanation. Assuming a set of angle-of-attack samples of $\alpha = [\alpha_1, \alpha_2, \ldots, \alpha_n]$ at free-stream Mach numbers of $M = [M_1, M_2, \ldots, M_m]$, the pitch moment response to each angle of α_i, where $i = 1, 2, \ldots, n$, at Mach numbers of M_j, where $j = 1, 2, \ldots, m$, is denoted as $A_\alpha(\mathrm{t}, \alpha_i, M_j)$. In these response simulations, $\alpha(t) = 0$ at $t = 0$ and is held constant at α_i for all $t > 0$. For a new angle of $\alpha^* > 0$ at a new free-stream Mach number of M^*, the responses of $A_\alpha(t, \alpha_k, M^*)$ are interpolated at $\alpha_k = [\alpha_1, \alpha_2, \ldots, \alpha_s]$, such that $0 < \alpha_1 < \alpha_2 < < \alpha_s$ and $\alpha_s = \alpha^*$. These angles can have a uniform or nonuniform spacing. The indicial functions of $C_{j\alpha k}$ for $k = 1, \ldots, s$ at each interval of $[\alpha_{k-1}, \alpha_k]$ are defined as

$$C_{j\alpha_1} = \frac{A_\alpha(t,\ \alpha_1,\ M^*) - C_{j0}(M^*)}{\alpha_1} \tag{3}$$

and

$$C_{j\alpha_k} = \frac{A_\alpha(t,\ \alpha_k,\ M^*) - A_\alpha(t,\ \alpha_{k-1},\ M^*)}{\alpha_k - \alpha_{k-1}}, \tag{4}$$

where C_{j0} denotes the zero-angle-of-attack pitch moment coefficient. The interval indicial functions are then used to estimate the values of the first integrals in Equations 1 and 2. These steps can easily be followed for a negative angle of attack, i.e., $\alpha^* < 0$. The functions of $C_{L\alpha}(t, \alpha, M)$, $C_{m\alpha}(t, \alpha, M)$, $C_{Lq}(t, \alpha, M)$, and $C_{mq}(t, \alpha, M)$ are unknown and will be determined in this article using CFD with a grid-motion approach, along with a time-dependent surrogate model.

CFD solver

The flow solver used for this study is the commercially-available flow solver Cobalt (Strang, Tomaro, and Grismer 1999), which solves the unsteady, three-dimensional, and compressible Navier–Stokes equations in an inertial reference frame. These equations in integral form are

$$\frac{\partial}{\partial t}\iiint \mathbf{Q}\, dV + \iint \left(\mathbf{f}\hat{i} + \mathbf{g}\hat{j} + \mathbf{h}\hat{k}\right).\hat{n}\, dS = \iint \left(\mathbf{r}\hat{i} + \mathbf{s}\hat{j} + \mathbf{t}\hat{k}\right).\hat{n}\, dS, \tag{5}$$

where V is the volume of the fluid element; S is the surface area of the fluid element; $\hat{n}$ normal to S; $\hat{i}, \hat{j}$, and $\hat{k}$ are the Cartesian unit vectors; and $\mathbf{Q} = (\rho, \rho u, \rho v, \rho w, \rho e)^T$ is the vector of conserved variables, where ρ represents air density, u, v, and w are velocity components, e is the specific energy per unit volume, and the superscript T denotes the transpose operation (Da Ronch et al. 2012). The vectors of $\mathbf{f}$, $\mathbf{g}$, and $\mathbf{h}$ represent the inviscid components:

$$\begin{aligned} \mathbf{f} &= \left[\rho u, \rho u^2 + p, \rho uv, \rho uw, u(\rho e + p)\right]^T, \\ \mathbf{g} &= \left[\rho v, \rho v^2 + p, \rho vu, \rho vw, v(\rho e + p)\right]^T, \\ \mathbf{h} &= \left[\rho w, \rho w^2 + p, \rho wu, \rho wv, w(\rho e + p)\right]^T. \end{aligned} \tag{6}$$

The vectors of $\mathbf{r}$, $\mathbf{s}$, and $\mathbf{t}$ represent the viscous components:

$$\begin{aligned} \mathbf{r} &= \left(0, \tau_{xx}, \tau_{xy}, \tau_{xz}, u\tau_{xx} + v\tau_{xy} + w\tau_{xz} + kT_x\right)^T, \\ \mathbf{s} &= \left(0, \tau_{xy}, \tau_{yy}, \tau_{yz}, u\tau_{xy} + v\tau_{yy} + w\tau_{yz} + kT_y\right)^T, \\ \mathbf{t} &= \left(0, \tau_{xz}, \tau_{zy}, \tau_{zz}, u\tau_{xz} + v\tau_{zy} + w\tau_{zz} + kT_z\right)^T, \end{aligned} \tag{7}$$

where τ_{ij} are the viscous stress tensor components, T is the temperature, and k is the thermal conductivity. The ideal gas law and Sutherland's law close the system of equations, and the entire equation set is nondimensionalized by free-stream density and speed of sound (Strang, Tomaro, and Grismer 1999). The Navier–Stokes equations are discretized on arbitrary grid topologies using a cell-centered finite volume method. Second-order accuracy in space is achieved using the exact Riemann solver of Gottlieb and Groth (1998) and least-squares gradient calculations using QR and frequencies in a fraction of a few seconds of computational time without the need of running CFD tools again.

This article considers the development of ROMs based on indicial functions that allow the prediction of pitching and plunging responses of a fighter aircraft within the space of frequency, amplitude, and Mach number. The transient aerodynamic response to a step change in a forcing parameter, such as angle of attack or pitch rate, is an indicial function. Assuming that the indicial functions are known, the aerodynamic forces and moments induced in any arbitrary maneuver can be estimated in the time domain by means of the well-known Duhamel's superposition integral (Leishman and Nguyen 1989). The indicial functions can be derived from analytical, CFD, or experimental methods (Librescu and Song 2006). Limited analytical expressions of indicial functions exist for two-dimensional airfoils. For incompressible flows, Wagner (1925) was the first to detail the analytical unsteady lift of a thin airfoil undergoing a plunging motion using a single indicial function (the so-called Wagner's function), with its exact values known in terms of Bessel functions. For unsteady, compressible flows past two-dimensional airfoils, Bisplinghoff, Ashley, and Halfman (1996) have also described an exponential approximation to the exact solutions of indicial functions at different Mach numbers. However, these analytical expressions are not valid for aircraft configurations.

The efforts to estimate the indicial functions for aircraft configurations can be classified into two groups: the direct and the indirect methods. Leishman (1993) has presented an indirect technique for identifying indicial functions from aerodynamic responses due to harmonic motions. However, the derived indicial functions using indirect methods depend largely on the quality of motion, e.g., amplitude, Mach number, and frequency. Experimental tests are limited for high frequencies and Mach numbers, and practically nonexistent for direct indicial-function measurements. An alternative is to use CFD, but special considerations are required to simulate step responses in CFD. Singh and Baeder (1997) used a surface-transpiration approach to directly calculate the indicial response due to angle of attack using CFD. Ghoreyshi, Jirásek, and Cummings (2012) have also proposed an approach based on grid motion for CFD-type calculation of indicial functions. In this article, the indicial functions of aircraft are calculated using the CFD and grid-motion approach. For motions at low angles of attack and assuming incompressible flow, only a single indicial function with respect to each forcing parameter needs to be generated (Leishman and Crouse, 1989). For compressible and high-angle-of-attack flows, many indicial functions need to be generated for different Mach numbers and angles of attack. The generation of all these functions using CFD is expensive and makes the creation of ROMs time consuming. Note that these models are still much cheaper than a brute-force approach, because the ROMs based on indicial functions eliminate the need to repeat calculations for each frequency.

A cost-effective unsteady-aerodynamic model needs a mathematical description of indicial functions as a function of angle of attack and Mach number. However, this model is often unavailable for three-dimensional configurations. It is more common to use surrogate models, which are mathematical approximations of the true response of the system built using some observed responses. By building surrogate models using a few observed responses, the total cost of modeling is reduced. In this article, a surrogate model is used based on the kriging technique to model indicial functions as a function of angle of attack and Mach number. In this article, the creation of reduced-order unsteady-aerodynamic models using indicial functions is reviewed. Next, the flow solver and an approach for CFD calculation of indicial functions are described. A surrogate model, built using some observed responses, is then described to approximate indicial function at new Mach numbers and angles of attack. The created ROM and the surrogate model are then used for aerodynamic predictions of a generic fighter configuration. The aircraft geometry and validation of CFD predictions are presented. Finally, the validity of ROMs is assessed by comparison of the model output with time-accurate CFD simulations.

Formulation

Reduced-order aerodynamics modeling

The problem of predicting unsteady lift and pitch moment responses of a generic fighter to pitching and plunging motions is considered. Assuming these motions could be started from different Mach numbers, the Mach number is held constant during each motion—i.e., $\dot{V} = 0$. The unsteady and nonlinear aerodynamic models used in this work are based on aerodynamic indicial functions by using superposition integrals. Tobak and colleagues (Tobak and Chapman 1985; Tobak, Chapman, and Schiff 1984) and Reisenthel (Reisenthel 1997; Reisenthel and Bettencourt 1999) have detailed the superposition process for the modeling of unsteady lift and pitch moment from angle-of-attack and pitch-rate indicial functions. Following their work, the time responses in lift due to the step changes in angle of attack α and normalized pitch rate q are denoted as CL_{α} and C_{Lq}, respectively.

Tyssel, L. 2000b. The TRITET grid generation system. In *Proceedings of the 10th International Conference on Numerical Grid Generation in Computational Field Simulations,* 16–20 September, Forth, Crete, Greece, eds., International Society of Grid Generation.

Wagner, H. 1925. Über die Entstehung des dynamischen Auftriebes von Tragflügeln. *Zeitschrift für Angewandte Mathematik und Mechanik* 5 (1): 17–35.

Wright, J. R., and J. E. Cooper. 2008. *Introduction to aircraft aeroelasticity and loads*. Chichester, U.K.: John Wiley.

Acknowledgments

The authors appreciate the support provided by the Modeling and Simulation Research Center at the U.S. Air Force Academy. Mehdi Ghoreyshi also would like to thank the National Research Council/U.S. Air Force Office of Scientific Research for financial support. The computational mesh was generated by Adam Jirásek.

Acknowledgments are expressed to the Department of Defense High Performance Computing Modernization Program (HPCMP) for providing computational resources.